

Ataluren prevented bone loss induced by ovariectomy and aging in mice through the BMP-SMAD signaling pathway

Lijun Zeng^{a,e}, Ranli Gu^{a,e}, Wei Li^{b,e}, Yuzi Shao^{a,e}, Yuan Zhu^{a,e}, Zhengwei Xie^{c,*}, Hao Liu^{d,e,**}, Yongsheng Zhou^{a,e,***}

^a Department of Prosthodontics, Peking University School and Hospital of Stomatology, Beijing 100081, China

^b Department of Oral Pathology, Peking University School and Hospital of Stomatology, Beijing 100081, China

^c Peking University International Cancer Institute, Peking University Health Science Center, Peking University, 38 Xueyuan Lu, Haidian District, Beijing 100191, China

^d Central Laboratory, Peking University School and Hospital of Stomatology, Beijing 100081, China

^e National Center for Stomatology & National Clinical Research Center for Oral Diseases & National Engineering Research Center of Oral Biomaterials and Digital Medical Devices & Beijing Key Laboratory of Digital Stomatology & National Health Commission Key Laboratory of Digital Technology of Stomatology, Beijing 100081, China

ARTICLE INFO

Keywords:

Ataluren
hBMMSC
Osteogenesis
Osteoporosis
BMP-SMAD pathway

ABSTRACT

Both estrogen deficiency and aging may lead to osteoporosis. Developing novel drugs for treating osteoporosis is a popular research direction. We screened several potential therapeutic agents through a new deep learning-based efficacy prediction system (DLEPS) using transcriptional profiles for osteoporosis. DLEPS screening led to a potential novel drug examinee, ataluren, for treating osteoporosis. Ataluren significantly reversed bone loss in ovariectomized mice. Next, ataluren significantly increased human bone marrow-derived mesenchymal stem cell (hBMMSC) osteogenic differentiation without cytotoxicity, indicated by the high expression index of osteogenic differentiation genes (*OCN*, *BGLAP*, *ALP*, *COL1A*, *BMP2*, *RUNX2*). Mechanistically, ataluren exerted its function through the BMP-SMAD pathway. Furthermore, it activated SMAD phosphorylation but osteogenic differentiation was attenuated by BMP2-SMAD inhibitors or small interfering RNA of *BMP2*. Finally, ataluren significantly reversed bone loss in aged mice. In summary, our findings suggest that the DLEPS-screened ataluren may be a therapeutic agent against osteoporosis by aiding hBMMSC osteogenic differentiation.

1. Introduction

Osteoporosis is a prevalent bone loss disease caused by a disruption in the balance between bone formation and bone resorption that eventually brings about bone loss [1]. Currently, physicians mainly use osteoclast-inhibiting drugs to treat osteoporosis. The main categories are estrogens, bisphosphonates, and calcitriol, which favor the maintenance of bone mass by doubling of osteoclast inhibition [2,3]. However, these agents also cause adverse effects that limit their long-term use in osteoporotic patients, such as osteonecrosis of the jaw, and breast and uterine cancer [4,5]. Decreasing bone resorption in patients with severe

bone loss is insufficient for remedying their condition. There are few commercially available osteogenic drugs, including parathyroid hormones (PTHs). PTH affects bone remodeling by improving osteoblast proliferation and reducing its apoptosis [6]. However, in vivo osteogenesis peaks after 6–12 months of PTH analog therapy, after which the serum markers of osteoclast and osteoblast activity gradually return to baseline levels. This diminished osteoblast influence is one of the factors limiting the long-term clinical use of PTH analogs [7]. The development of new osteogenic agents for enhancing osteogenesis is a popular research direction.

Big data and deep learning have provided a new avenue for drug

* Correspondence to: Peking University International Cancer Institute, Peking University Health Science Center, Peking University, 38 College Road, Haidian District, Beijing 100191, China.

** Correspondence to: Central Laboratory, Peking University School and Hospital of Stomatology, 22 Zhongguancun South Avenue, Haidian District, Beijing 100081, China.

*** Correspondence to: Department of Prosthodontics, Peking University School and Hospital of Stomatology, 22 Zhongguancun South Avenue, Haidian District, Beijing 100081, China.

E-mail addresses: xiezhenwei@hsc.pku.edu.cn (Z. Xie), kqliuhao@bjmu.edu.cn (H. Liu), kqzhouysh@hsc.pku.edu.cn (Y. Zhou).

<https://doi.org/10.1016/j.bioph.2023.115332>

Received 18 May 2023; Received in revised form 2 August 2023; Accepted 13 August 2023

0753-3322/© 2023 Published by Elsevier Masson SAS. This is an open access article under the CC BY-NC-ND license (<http://creativecommons.org/licenses/by-nc-nd/4.0/>).

discovery. Repurposing drug function can rapidly reduce drug development costs and meet clinical needs [8]. The deep learning-based efficacy prediction system (DLEPS) is derived from Connectivity Map (CMAP), a web-based tool for screening compounds against various diseases using gene signatures [9,10]. This screening is attributed to comparing the DLEPS-predicted dataset with a user-selected phenotypic gene signature of interest using a high-resolution and high-specificity pattern matching algorithm [9]. In the present study, the gene signatures of osteoporosis are used from ArrayExpress, a public database for microarrays and high-throughput sequencing data, to screen compounds in D3680 by DLEPS. The search results in a series of compounds associated with gene expression patterns highly correlate with the phenotype of interest and are ranked according to the gene set enrichment score, which aids the search for new disease therapeutic agents or therapeutic targets.

Generally speaking, mesenchymal stem cells (MSCs) can differentiate toward osteogenic, chondrogenic, and lipogenic lineages [11]. MSC differentiation into osteoblasts can be promoted by activating signaling pathways of osteogenic differentiation. The activation of various classical signaling pathways, such as Wnt/ β -catenin [12], bone morphogenetic proteins (BMPs) [13–15] and Notch [16], upregulates the expression of transcription factors such as RUNX family transcription factor 2 (RUNX2) and Sp7 transcription factor (OSX), which in turn activate alkaline phosphatase (ALP) and osteocalcin (OCN) and promote mineralization [17–22].

We identified ataluren as a candidate for treating osteoporosis by DLEPS. Ataluren is a protein expression repair drug for treating muscle atrophy and dystrophy [23] which was ratified by the European Commission in 2014. It affects the ribosomal translation of early termination codon mRNA with several advantages include minimal adverse effects and long-term use in patients aged ≥ 5 years [24–26]. However, its function in bone stabilization has not been discovered yet. Meanwhile, it remains unknown whether ataluren can influence bone marrow-derived MSC (BMMSC) function via the osteogenic signaling pathway.

Therefore, in the present study, we evaluated the role of ataluren in reversing bone loss in ovariectomized (OVX) mice and explored its effects and underlying mechanisms on osteogenic differentiation of human BMMSC (hBMMSC) *in vitro*. Moreover, we used aged mouse models to investigate the therapeutic effects of age-related bone loss in depth.

2. Materials and methods

2.1. Data Collection

Microarray database reference datasets were downloaded from the ArrayExpress database (accession number E-GEOD-35959; available from <https://www.ebi.ac.uk/arrayexpress/experiments/E-GEOD-35959>) by searching for osteoporosis, for which we obtained the gene expression profiles of 19 human MSC donors.

2.2. Small-molecule Libraries

In this research, a natural compound library and an FDA-approved library merged as D3680 (TargetMol, $n = 3680$), were used to discover novel osteoporosis treatment agents.

2.3. Drug Repositioning

DLEPS was used for calculating the anti-osteoporosis score using the differentially expressed genes (DEG) as previous described [9]. DLEPS was trained applying chemically induced changes in transcriptional profiles from the L1000 [27]. Compounds are processed by RDKit (version 2017.9.1) into a standard system input linear simplified molecular (Simplified molecular-input line-entry system, SMILES), which are parsed into a Grammar variational autoencoder (GVAE) grammar

tree (76 node types), then parsed into flattened vectors, converted into single heat arrays, afterwards passed to a three-layer one-dimensional convolutional neural networks (CNN), flattened output fragments ($\text{dim} = 2510$), passed to the dense layer, and output average vectors ($\text{dim} = 56$) and radius vector ($\text{dim} = 56$), encoding a sphere in a high-dimensional space¹³. The coordinates of a randomly sampled point ($\text{dim} = 56$) in this sphere were selected as the latent vector and then passed through a five-layer dense network to predict changes in the transcriptional profile [28]. Enrichment scores for 110 up-regulated genes and 135 down-regulated genes were used to calculate the osteoporosis effective score. After input the list of up- and down-regulated genes, we obtained the ranking scores of these chemicals, from which the top-ranked molecules were selected.

2.4. Culture, osteogenic induction of hBMMSCs

Primary hBMMSCs were acquired from ScienCell and cultivated in proliferation medium (PM) [α -minimum essential medium (α -MEM, Gibco) containing 10% (v/v) fetal bovine serum (FBS, ExCell Bio) and 1% (v/v) penicillin streptomycin (Gibco)]. Cells were expanded to the 5th and 6th generation for experiments. The osteogenic differentiation medium (OM) contained α -MEM with 10% (v/v) FBS, 1% (v/v) penicillin streptomycin, 10 nM dexamethasone (Sigma), 200 μM vitamin C (Sigma), and 10 mM β -glycerophosphate (β GP, Sigma).

2.5. Concentrated ataluren solution preparation

28.5 mg ataluren (CSNpharm) was dissolved in 1 mL DMSO (Sigma) and blown repeatedly, after that, 9 mL α -MEM was added slowly to yield a concentrated solution of 10 mM. Then, α -MEM was slowly added and diluted to 0.1 mM ataluren stock solution. This was divided and used to detect the role of gradient concentrations of ataluren on hBMMSC differentiation and to select the best concentration for promoting osteoblastic differentiation.

2.6. Cytotoxicity

The cytotoxicity of ataluren was determined by the CCK-8 assay. Briefly, cells were inoculated at 2000 cells/well in clear, flat-bottomed, 96-well plates. Cells were then cultured in PM, or in PM with 10, 50 and 100 μM ataluren. Cells from three wells of the same treatment were tested daily from day 1 to day 7 to determine the cytotoxicity of the relevant reagents by the CCK-8 assay. The cultures were then removed from the incubator and the absorbance at 460 nm was read.

2.7. Staining and quantification of alkaline phosphatase (ALP) and alizarin red S (ARS)

Early markers of osteoblast differentiation in the hBMMSCs were examined with ALP staining and quantitative determination of ALP activity. Late markers of osteoblast differentiation were examined using ARS staining and semi-quantitative determination of mineralization. ALP staining was performed using an NBT/BCIP staining kit (CoWin Biotech) according to the manufacturer's guidelines on day 7 after OM induction. ALP activity was tested with an ALP assay kit (Nanjing Jiancheng Bioengineering Institute). The ALP activity was calculated based on the absorbance in 520 nm.

Fourteen days after OM induction, the hBMMSCs were stained with 2% ARS buffer (Sigma). Mineral accumulation was quantitated using 100 mM cetylpyridine solution (Sigma) in a multi-well sample plate. Mineral accumulation was quantitated based on the absorbance in 490 nm.

2.8. Western blot analysis

The hBMMSCs were cultured in 60-mm dishes and incubated with 1

× radioimmunoprecipitation assay lysis buffer (Huaxingbio) containing a mixture of PMSF (Huaxingbio) and protease inhibitor (Huaxingbio). After centrifugation on ice, the protein concentration in the supernatant was measured by the bicinchoninic acid approach. The same amount of protein was split on a 10% sodium dodecyl sulfate-polyacrylamide gel and transferred onto a PVDF membrane (Millipore). The membranes were incubated in rapid blocking solution to block nonspecific binding, then incubated with primary antibodies against BMP2 (Abcam, ab214821, 1:1000), RUNX2 (Abcam, ab264077, 1:1000), OSX (Abcam, ab229258, 1:1000), SMAD1/5 (Abcam, ab80255, 1:1000), pSMAD1/5 (Cell Signaling Technology, 9516, 1:1000), or GAPDH (Abcam, ab9485, 1:2500). Primary antibody had been used 4 µL. Then, the membranes were incubated with the secondary antibody for 1 h. Finally, the immunoreacted protein bands were detected by enhanced chemiluminescence.

2.9. Quantitative real-time PCR (qRT-PCR)

Total cellular RNA was extracted from the hBMMSCs with TRIzol (Invitrogen) according to the manufacturer instruction manual. Complementary DNA (cDNA) was reverse-transcribed using a PrimeScript RT Reagent Kit (Takara). qRT-PCR was performed with SYBR Green Master Mix (YEASEN) on an ABI Prism 7500 RT-PCR System. The gene index was standardized to the GAPDH index, which was used as the house-keeping gene. The primer sequences used are presented in Table S1. Each sample was taken in triplicate and fluorescence data was collected at the end of each cycle.

2.10. RNA sequencing

RNA of each group was extracted as described above. Library preparations were conducted using NEBNext® Ultra™ RNA Library Prep Kit for Illumina® (New England Biolabs) and subjected to Illumina sequencing. We quantified the gene expression (featureCounts, 1.5.0-p3) level of each sample separately and then combined to obtain the expression matrix of all samples [29]. FPKM was successively corrected for sequencing depth and gene length [30]. DEGs between the OM and ATA groups were screened by DESeq2 (Anders et al., 1.20.0). $|\log_2(\text{FoldChange})| > 0$ & $p \text{ value} \leq 0.05$ were considered statistically significant for DEGs. To elucidate the underlying biological processes and explore the molecular mechanisms associated with differentially expressed products, we performed gene ontology (GO) enrichment analysis by clusterProfiler (3.8.1) to predict promising signaling pathways associated with differentially expressed genes.

2.11. Small interfering RNA (siRNA) transfection

BMP2-targeting siRNAs and Scramble siRNA were acquired from Sangon Biotech. The siRNA sequences were as follows: sense, GAUCAUCUGAACUCCACUAAUTT and antisense, AUUAGUGGAGUUCAGAUGAUCTT. 24 h prior to treatment, hBMMSCs were inoculated at 80,000 cells/well in 24-well plates. Cells were treated with siBMP2 or scramble in 300 µL of Opti-MEM (Gibco) containing 1 µL of lipo-2000 (Invitrogen) for 4 h. Thereafter the medium was changed to PM. The cells were transfected with siBMP2 and harvested for RNA analyses and western blotting (WB) after 2 days. For osteogenic induction, the cells were transfected every 5 days in OM and harvested after 1 week.

2.12. Animals and experimental design and ethical statement

Female C57BL/6 mice were obtained from Charles River Laboratory Animal Technology Co., Ltd. They were housed in specific pathogen-free conditions at the Animal Center of Peking University School and Hospital of Stomatology. This study was authorized by the Peking University School of Medicine Institutional Committee for Animal Care and Use (LA2021040).

In vivo metabolism studies of ataluren suggested that the administration of ataluren in mice was by gavage at a concentration of 20 mg/mL and a gavage dose of 15 mL/kg. Based on a mouse weight of 24–34 g, we can calculate the administered dose as 300 mg/kg [31].

Estrogen deficiency-induced bone loss model for primary validation: Twenty-five mice (56 days old) were placed in five groups ($n = 5$). After general anesthesia, bilateral OVX or sham surgery was performed with standardized techniques. Four weeks after surgery, 300 mg/kg/d ataluren (20 mg/mL, Macklin) mixed in 0.5% Carboxymethylcellulose (CMC, Sigma), 36.4 mg/kg/d natamycin (NATA, 15 mg/mL, Solarbio) mixed in 0.5% CMC and 0.26 mg/kg/d prucalopride (PRU, 0.0173 mg/mL, Mitachieve) mixed in 0.5% CMC was administered by gavage for 2 months (once every other day). The five groups were: (1) SHAM+CMC, (2) OVX+CMC, (3) OVX+ATA, (4) OVX+NATA, and (5) OVX+PRU.

Estrogen deficiency-induced bone loss model: Twenty mice (56 days old) were placed in four groups ($n = 5$). Four weeks after OVX or sham surgery, 300 mg/kg/d ataluren mixed in 0.5% CMC was administered by gavage for 2 months (once every other day). The four groups were: (1) SHAM+CMC, (2) SHAM+ATA, (3) OVX+CMC, and (4) OVX+ATA.

Age-related bone loss model: Ten mice (18 months old) were stochastically divided into two groups ($n = 5$): (1) Aged+CMC and (2) Aged+ATA. 300 mg/kg/d ataluren (20 mg/mL, Macklin) mixed in 0.5% CMC (Sigma) was administered by gavage for 2 months (once every other day).

All mice were euthanized, and the left femurs were collected and fixed in 10% formalin. The right femur was also collected and preserved in 10% formalin away from light. The serum was also collected from each mouse. The major organs were carefully collected and fixed in 10% formalin for H&E staining of tissue sections to observe the tissue toxicity of ataluren.

2.13. Serum enzyme-linked immunosorbent assay (ELISA)

Serum PINP and serum CTX-1 were used as markers of bone formation and bone resorption, respectively. The serum biomarkers were tested using an ELISA kit (Jiangsu Meimian Industrial Co., Ltd.).

2.14. Bone histomorphology

Bone histomorphology analyses were performed according to a previously described protocol [32]. For the measurement of dynamic bone parameters, the mice were injected with calcein (10 mg/kg body weight) and alizarin-3-methyliminodiacetic acid (10 mg/kg body weight) at 7 and 2 days before euthanasia, respectively. After euthanasia of the mice, the right femur was removed and stored away from light, dehydrated, and embedded for hard tissue sectioning. The double-labeling in the bone tissue was observed under fluorescence microscopy, and quantitative analysis was performed using Image J (National Institutes of Health). Mineral apposition rates (MAR) represents the rate of new bone formation.

The left femurs were carefully collected and fixed in 10% formalin, dehydrated in 70% ethanol and embedded in methyl methacrylate. The femur was cut in half at the mid-axis and sectioned in the transverse plane of a 200 µm thick section for H&E staining and observed under the microscope.

2.15. Micro-computed tomography

Femoral specimens were scanned by the Inveon MM System (Siemens) micro-computed tomographer following previously established protocols [33]. The scanning parameters were as follows: an effective pixel size of 8.89 µm, a voltage of 60 kV, a current of 220 µA, and an exposure time of 1500 ms during each of the 360 rotational steps. The resulting images comprised 1536 slices and possessed a voxel size of 8.89 µm in all three dimensions. The 3D visualization images were reconstructed using two-dimensional images, and the parameters were

calculated using the Inveon Research Workplace (Siemens) software. The parameters included bone mineral density (BMD), bone volume/total volume (BV/TV), trabecular number (Tb.N), bone surface area/bone volume (BS/BV), trabecular separation (Tb.Sp), and trabecular thickness (Tb.Th). These parameters were measured in regions of interest (ROI) of femur (0.5–3 mm below the distal growth plate) as previously described according to guidelines set by the American Society for Bone and Mineral Research [34–36].

2.16. Statistical analysis

All data are expressed as the mean \pm standard deviation (SD) of at least 3 experiments per group. Firstly, we performed the Shapiro-Wilk normality test to check the normal distribution of the groups. If the normality test was passed, a student t-test was conducted. If the normality test was failed, a Mann-Whitney test was used in two groups. In order to compare multiple groups, one-way ANOVA was used if the normality test was passed, and then Tukey's multiple comparison test was conducted via SPSS 23.0 (SPSS Inc.). $P < 0.05$ and < 0.01 indicated statistical significance.

3. Results

3.1. Ataluren prevents bone loss in OVX mice

First, we identified the up-/down-regulated genes of primary osteoporosis and advanced age on human MSCs (E-GEOD-35959) [37] (Table S2 for the list of genes). DLEPS is a tool that uses changes in gene expression profiles in diseased states and candidate compounds as inputs to complete predictions. Next, the up-/down-regulated genes were used as DLEPS input (REF <https://www.nature.com/articles/s41587-021-00946-z>) to calculate the efficacy score using the D3680 library (Table S3). We identified many small molecules that could yield new ideas for therapeutic research on osteoporosis. The results of the DLEPS screening are shown in the scatter plot (Fig. 1a), the top points in the ranking of the effective scores for osteoporosis are concentrated in the upper right corner. The scores of the top-ranked compounds for osteoporosis therapy are shown in a heat map (Fig. 1b). After screening the literature library of Pubmed, we excluded the following compounds owing to reported osteoporosis therapeutic effects and toxic side effects of top-ranked compounds from heat map. For example, tideglusib, coumarin, and dydrogesterone promote the regeneration of bone defects [38–40]. However, zoxazolamine and phenacetin have considerable biological toxicity and limit their clinical application [41,42]. After that, only ataluren, natamycin, and prucalopride from heat map was left for further analysis.

Ataluren (ATA), natamycin (NATA), and prucalopride (PRU) were selected for micro-computed tomography (micro-CT) examination of whether they can reverse bone loss in OVX mice. Fig. S1a shows representative micro-CT and hematoxylin-eosin (H&E) staining images of OVX mouse femur. Ataluren improved bone mineral density (BMD) and bone microarchitecture comparable to that of the SHAM+CMC (carboxymethyl cellulose) group and was superior to that of the natamycin and prucalopride groups (Fig. S1b). Our results show that among the three drug candidates, ataluren induced the best reversal of bone loss in the OVX mice. Therefore, ataluren was selected for further study.

To confirm the effect of ataluren on inhibiting bone loss, we compared the morphological and H&E staining images of the femur and bone morphological parameters in four groups of mice (8 months old): SHAM+CMC (sham surgery plus gavage CMC, $n = 5$), SHAM+ATA (sham surgery plus gavage ataluren, $n = 5$), OVX+CMC (OVX surgery plus gavage CMC, $n = 5$), and OVX+ATA (OVX surgery plus gavage ataluren, $n = 5$) (Fig. 1c, Fig. S2 and S3). The OVX+ATA mice had higher BMD, bone volume/total volume (BV/TV), trabecular thickness (Tb.Th), and trabecular bone number (Tb.N) ($p < 0.01$, $p < 0.01$, $p < 0.05$, $p < 0.01$, respectively) and lower trabecular spacing (Tb.Sp)

compared with the OVX+CMC group ($p < 0.01$). Of note, BMD, BV/TV, and Tb.N were also significantly increased in SHAM+ATA mice compared to the SHAM+CMC group ($p < 0.05$, $p < 0.05$, $p < 0.01$, respectively) (Fig. 1e). New bone formation in the distal femoral epiphysis was evaluated by dual labeling with calcein and alizarin-3-methyliminodiacetic acid. There was greater MAR in the OVX+ATA mice compared to the OVX+CMC mice ($p < 0.01$). Besides, the MAR of SHAM+ATA group was higher than that of SHAM+CMC group ($p < 0.01$) (Fig. 1d, f, and Fig. S4), indicating that ataluren promoted bone formation in OVX+ATA and SHAM+ATA group. Additionally, ataluren significantly increased levels of the serum bone formation marker P1NP (propeptide of type I collagen) ($p < 0.05$) (Fig. 1g) and decreased levels of the bone resorption marker CTX-1 (C-terminal telopeptide of type I collagen) ($p < 0.05$) (Fig. 1h). Although P1NP was increased in OVX mice, their CTX-1 values were also significantly increased, indicating that the imbalance in bone metabolism was more severe in OVX mice. These results demonstrate that ataluren significantly recovers bone loss with better trabecular structure and higher bone volume in OVX mice.

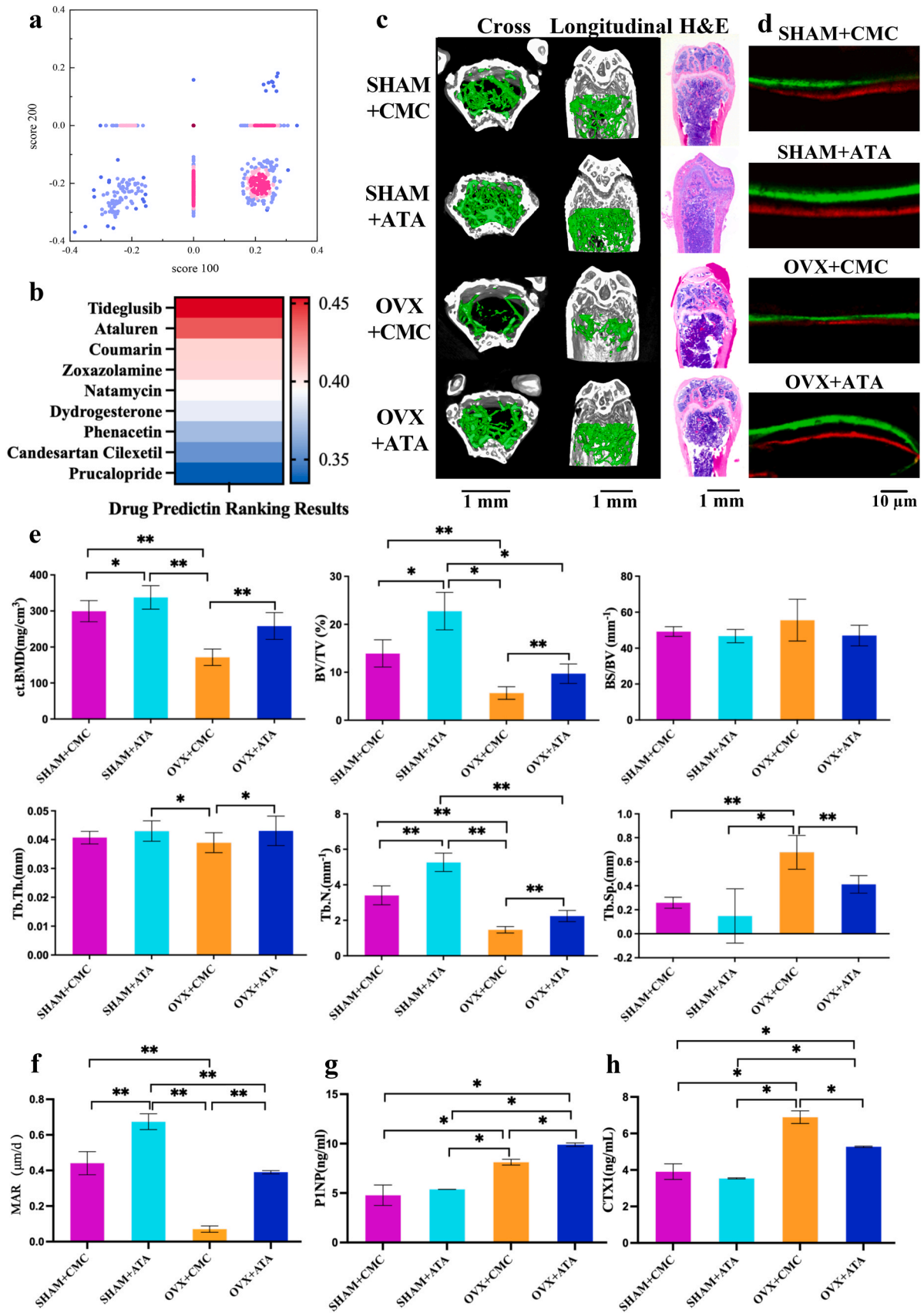
3.2. Ataluren promotes hBMMSC osteogenic differentiation in vitro

We used hBMMSCs as a model system for uncovering the potential effects of ataluren on bone formation. We examined ataluren cytotoxicity by using the Cell Counting Kit-8 (CCK-8) assay to explore its effects on hBMMSC proliferation. The CCK-8 curves showed that, from day 4–7, cells treated with 1% dimethyl sulfoxide (DMSO) and 10 μ M and 50 μ M ataluren showed no significant difference in cell proliferation capacity compared with cells treated with proliferation medium (PM) (Fig. 2a). Cell proliferation capacity was partially inhibited by 100 μ M ataluren, indicating less than 50 μ M may be a safe usage.

The effect of ataluren on hBMMSC osteogenic differentiation was determined using ALP and alizarin red S (ARS) staining and quantitative analysis. Ataluren (10 μ M, 50 μ M) increased ALP activity compared with the OM (osteogenic medium) group ($p < 0.05$, Fig. 2b, c), and 50 μ M was more effective than 10 μ M. ARS staining showed that 10 and 50 μ M ataluren increased mineralized nodules in the hBMMSCs as compared with the OM group ($p < 0.05$, respectively) and 50 μ M have a better effect (Fig. 2d, e). Furthermore, the mRNA expression levels of RUNX2, an osteogenic differentiation marker, were significantly increased in hBMMSCs treated with 10 and 50 μ M ataluren compared with OM group ($p < 0.01$) (Fig. 2f). WB results showed that 10 and 50 μ M ataluren significantly elevated RUNX2 and OSX protein levels as compared with that in the OM group ($p < 0.01$, respectively) (Fig. 2g, h). However, the addition of ataluren to the PM did not promote hBMMSC osteogenic differentiation. Moreover, the addition of 1% DMSO to the PM or OM had no promoting effects on osteogenesis (Fig. S5).

3.3. Ataluren promotes hBMMSC osteogenic differentiation through BMP-SMAD signaling pathway activation

We performed RNA sequencing (RNA-seq) on ataluren-treated hBMMSCs to systematically examine how it affects global transcriptional changes. Ataluren (50 μ M) upregulated 133 genes and down-regulated 383 genes compared to the OM group (Fig. 3a). Among the upregulated genes, the most significantly expressed gene was *DUSP5* ($p < 0.001$) (Fig. 3b). A detailed list of up-regulated genes can be found in the Table S4. *DUSP5* has been suggested to enhance MSC osteogenic differentiation through the BMP-SMAD pathway [43]. Gene ontology (GO) enrichment analysis showed enrichment of the BMP signaling pathway (Fig. 3c). Accordingly, we hypothesized that ataluren promotes osteogenesis by activating the BMP-SMAD pathway. To understand the potential molecular mechanisms by which ataluren promotes hBMMSC differentiation into osteoblasts, BMP-SMAD signaling pathway activation was investigated by qRT-PCR and WB. In order to assess the



(caption on next page)

Fig. 1. Ataluren prevents bone loss in OVX mice. **a** Scatter plot was generated to compare the efficacy scores of osteoporosis at 200 (y-axis) and 100 (x-axis), which made by DLEPS based on osteoporosis differential genes. Subsequently, the computationally predicted molecules for osteoporosis treatment in the second quadrant were chosen for experimental investigation. The density from low to high of the dots on the scatter plot was represented by a color gradient ranging from blue to red. **b** Heat map of the top nine predicted drugs. The transition from red to blue indicated that the ranking score goes from high to low. **c** Micro-CT (left) and H&E (right) staining images of femurs among SHAM+CMC, SHAM+ATA, OVX+CMC, and OVX+ATA groups. Micro-CT images are at a scale of 1 mm. Scale bar = 1 mm. **d** Representative images of new bone formation in the distal femoral epiphysis assessed by double-labeling with calcein and alizarin-3-methyliminodiacetic acid. Scale bar = 10 μ m. **e** Bone morphometry analysis among 4 groups. **f** MAR of SHAM+CMC, SHAM+ATA, OVX+CMC, and OVX+ATA. **g** Serum levels of P1NP. **h** Serum levels of CTX-1. All data shown are the mean \pm SD in **e**, **f**, **g**, and **h**, $n = 5$. * $P < 0.05$, ** $P < 0.01$ by ANOVA. MAR: Mineral apposition rates.

osteogenic abilities of hBMMSCs at the gene level, we screened the osteogenic gene markers BMP2, COL1A, ALP, BGLAP, and OSX [44,45]. Detailedly, ALP and COL1A were early osteoblast differentiation markers, and BGLAP was late one [46]. Mature BMPs bind to their receptor to induce SMAD1/5/9 phosphorylation, leading to expression of master osteogenic regulators RUNX2 and OSX, and effector proteins ALP [47]. The qRT-PCR results demonstrated that 50 μ M ataluren remarkably increased the mRNA expression levels of *BMP2*, *COL1A*, *ALP*, *BGLAP*, and *OSX* compared with OM ($p < 0.05$ or $p < 0.01$, respectively) (Fig. 3d). Moreover, it activated genes downstream of the SMAD signaling pathway during osteogenesis in hBMMSCs (Fig. 3e). That is, ataluren upregulated phosphorylated SMAD1/5, RUNX2, OSX, and BMP2 ($p < 0.01$, respectively, Fig. 3f).

3.4. Inhibition of the BMP-SMAD pathway blocks ataluren-induced hBMMSC osteogenic differentiation

We blocked BMP-SMAD signaling with the TGF- β -SMAD inhibitor LDN-193189 HCl and used small interfering RNA (siRNA)-mediated gene silencing targeting *BMP2* (siBMP2) to verify if ataluren regulates osteoblast differentiation via BMP-SMAD pathway. The increased ALP activity was blocked after BMP-SMAD pathway had been inhibited by siBMP2 and LDN-193189 HCl (both, $p < 0.01$) (Fig. 4a, c). The increase in calcium nodules, measured by ARS staining, was also blocked by LDN-193189 HCl and siBMP2 as compared with the 50 μ M ataluren treatment group or the Scramble+ 50 μ M ataluren group (both, $p < 0.01$) (Fig. 4b, d). WB and quantification showed that the increase in SMAD1/5 phosphorylation (both, $p < 0.01$) and the osteogenic marker RUNX2 (both, $p < 0.01$) was inhibited in the presence of LDN-193189 HCl, siBMP2, or both (Fig. 4e, f). These results confirm that ataluren induced a positive osteogenic promoting effect in hBMMSCs through the BMP-SMAD pathway. Moreover, the addition of LDN-193189 HCl and siBMP2 to the PM had no effects on ALP and ARS staining. (Fig. S6).

3.5. Ataluren partially reverses bone loss in aged mice

To explore if ataluren is effective in naturally aged mice, 18-month-old mice were treated with ataluren and their bone mass and bone density were measured by the micro-CT, H&E staining, and Masson staining of the femur. The results exhibited that ataluren significantly increased BV/TV and Tb.Th (both, $p < 0.01$) and decreased Tb.Sp ($p < 0.01$) as compared with the Aged+CMC mice (Fig. 5a, c, and Fig. S7). MAR was visualized with calcein and alizarin-3-methyliminodiacetic acid. As expected, the new bone formation rate was meager in the Aged+CMC mice. In contrast, the ataluren-treated mice had greatly restored new bone formation capability ($p < 0.01$) (Fig. 5b, d, and Fig. S8). Furthermore, ataluren treatment significantly decreased CTX-1 levels ($p < 0.05$) (Fig. 5e) and increased P1NP levels ($p < 0.05$) (Fig. 5f). These results indicate that ataluren can partially reverse bone loss in aged mice.

To explore the safety of ataluren, we treated sham control mice (8 weeks) and aged mice with 20 mg/mL ataluren for 2 months. There were no toxic side effect changes in the heart, spleen, liver, lungs, or kidneys of the ataluren-treated mice (Fig. S9).

4. Discussion

In the present study, the underlying anti-osteoporotic effect of ataluren was predicted by DLEPS firstly. Moreover, ataluren lessened OVX-related and aged-related bone loss, which probably due to promoting hBMMSC osteogenic differentiation dependent on the BMP-SMAD pathway.

Currently, drug-related research and development benefit from advances in biotechnology and computer science. Various algorithms, software, and tools continue to emerge from the analysis and summary of large amounts of experimental data. The gene expression profiles in disease reveal potential changes in gene activity which contribute to illness and enable targeted therapeutic interventions [48–50]. Deep learning algorithms were widely used in drug screening. Hajjo et al. algorithmically discovered that the SERM analogue raloxifene can act on the Alzheimer's target 5-HT6R [51]. Wang et al. entered target-ligand feature vector pairs and eventually output binary interaction predictions and screened potential drugs for the treatment of type II diabetes [52]. A recent study discovered structurally unique antibacterial molecules through a deep learning approach [53]. Previous studies focused on targets [52,54,55], but many diseases or biological processes lack clear targets. Therefore, in the present study, we examined the gene expression profiles of human MSCs from the ArrayExpress database for senescence (GSE35956), primary osteoporosis (GSE35957), and cellular senescence (GSE35958). Then, we used DLEPS to identify small bio-active molecules capable of reversing the genetic changes in osteoporosis.

As shown in Fig. 1c (ct.BMD, BV/TV, Tb.N), Fig. 1f (MAR) and Fig. 1g, ataluren increases bone mass by improving bone formation, even in untreated mice (SHAM+ATA vs SHAM+CMC). Usually, BS/BV increases in the early stage of bone resorption. In this study, OVX mice showed complete resorption of bone trabeculae, and the decrease of both BS and BV. Compared with the OVX+CMC group, BS/BV difference was not statistically significant (Fig. 1c), while BV/TV and Tb.N (Fig. 1c) were significantly higher in OVX+ATA group, which demonstrated that ataluren promoted osteogenesis by increasing bone regeneration (BS and BV increase simultaneously) rather than by inhibiting bone resorption (BS decreases while BV increases). Therefore, our subsequent study focused on ataluren which promotes osteogenic differentiation in hBMMSCs. Moreover, the fact that ataluren improved bone formation in both young and old animals indicated that the efficacy of ataluren is not age-dependent. In bone microenvironment of healthy person, the processes of osteogenesis and osteolysis exhibit a dynamic equilibrium. However, our research exhibited that ATA plays an excellent effect on osteogenesis through the BMP-SMAD pathway in vitro and vivo. Hence, the augmentation of bone volume occurs due to the predominance of osteogenesis over osteolysis, which may be the reason on increased bone mass induced by ATA in untreated mice. In conclusion, we have found the osteogenesis-promoting effect of ataluren for the first time.

During protein integration, nonsense mutations in the premature termination codon produce a truncated, inactive protein product. This defective gene product causes many diseases, including muscular dystrophy, cystic fibrosis, and some cancers [56–58]. ataluren is a small-molecule nonsense repressor that stimulates stop codon reading and thereby acts as a treatment for these diseases [59]. The addition of Stop-POST5 (containing the UGA stop codon at the A-site) is shifted to extension. Ataluren cannot provoke foundational read-through in

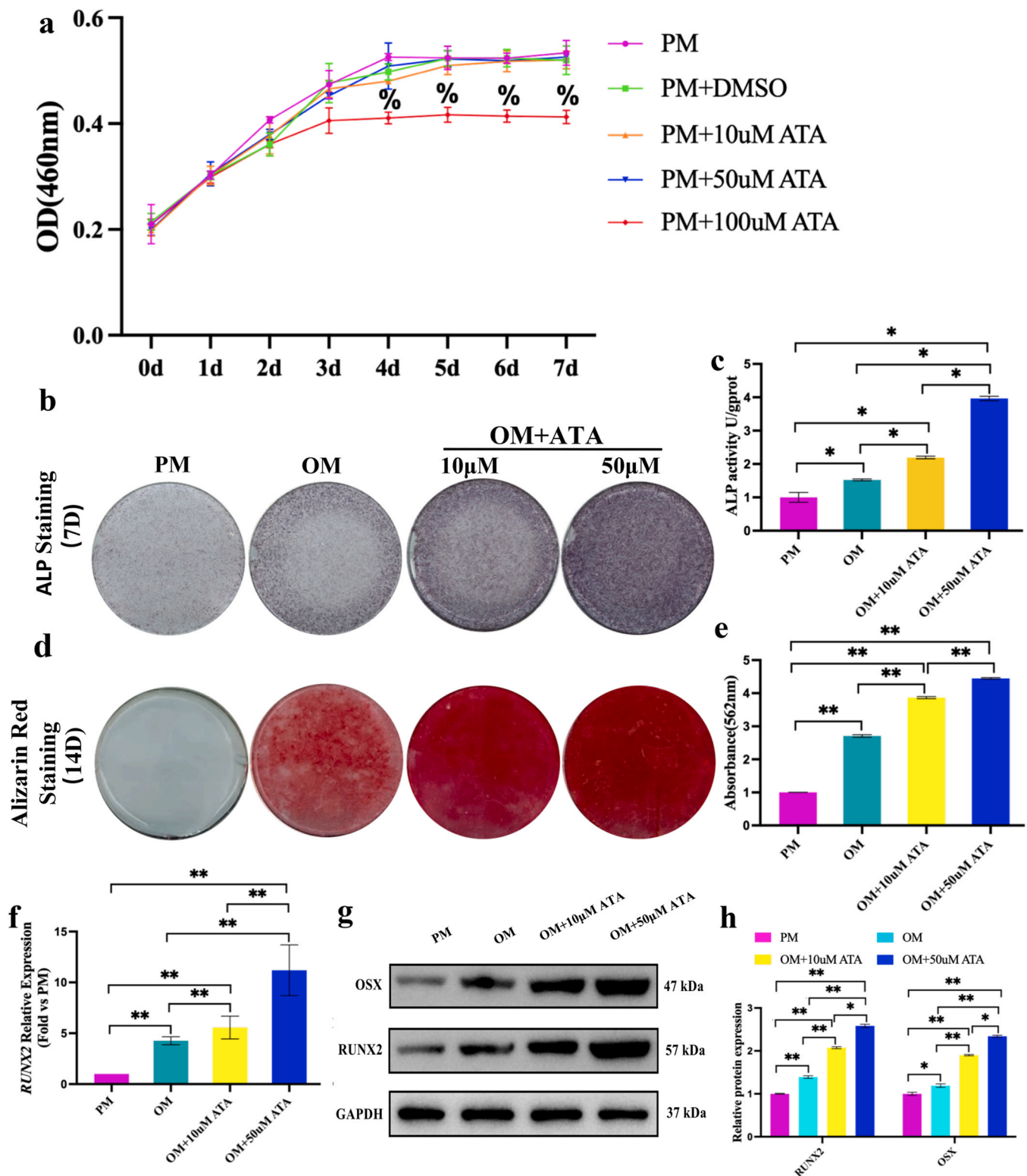


Fig. 2. Ataluren promotes hBMMSC osteogenic differentiation in vitro. **a** CCK-8 proliferation curve of hBMMSCs in PM, PM+DMSO, and PM+ATA (10, 50, and 100 μ M). **b** ALP staining of hBMMSCs in PM, OM, and OM+ATA (10, 50 μ M). **c** ALP activity quantification. **d** ARS staining of hBMMSCs in PM, OM, and OM+ATA (10, 50 μ M). **e** ARS semi-quantification results. **f** qRT-PCR results for *RUNX2*. **g** WB analysis of *RUNX2*, *OSX*, and the internal control *GAPDH*. **h** Quantitative analysis of *OSX*/*GAPDH* and *RUNX2*/*GAPDH*. All data shown are the mean \pm SD in **b**, **d**, **e**, and **g**, $n = 3$. * $P < 0.05$, ** $P < 0.01$ by ANOVA.

eRF1/eRF3 deficiency [60]. A likely target of ataluren is the ribosome, which produces full-length proteins by facilitating the insertion of near-homologous tRNAs at nonsense codon sites, with no apparent effect on transcription, mRNA processing, or mRNA or protein stability [61].

There is little direct evidence that ataluren promotes hBMMSC osteogenic differentiation. Only one study has shown that ataluren can treat mucopolysaccharidosis type VI, whose clinical characteristic is multiple bone dysplasia, by restoring arylsulfatase B deficiency and improving

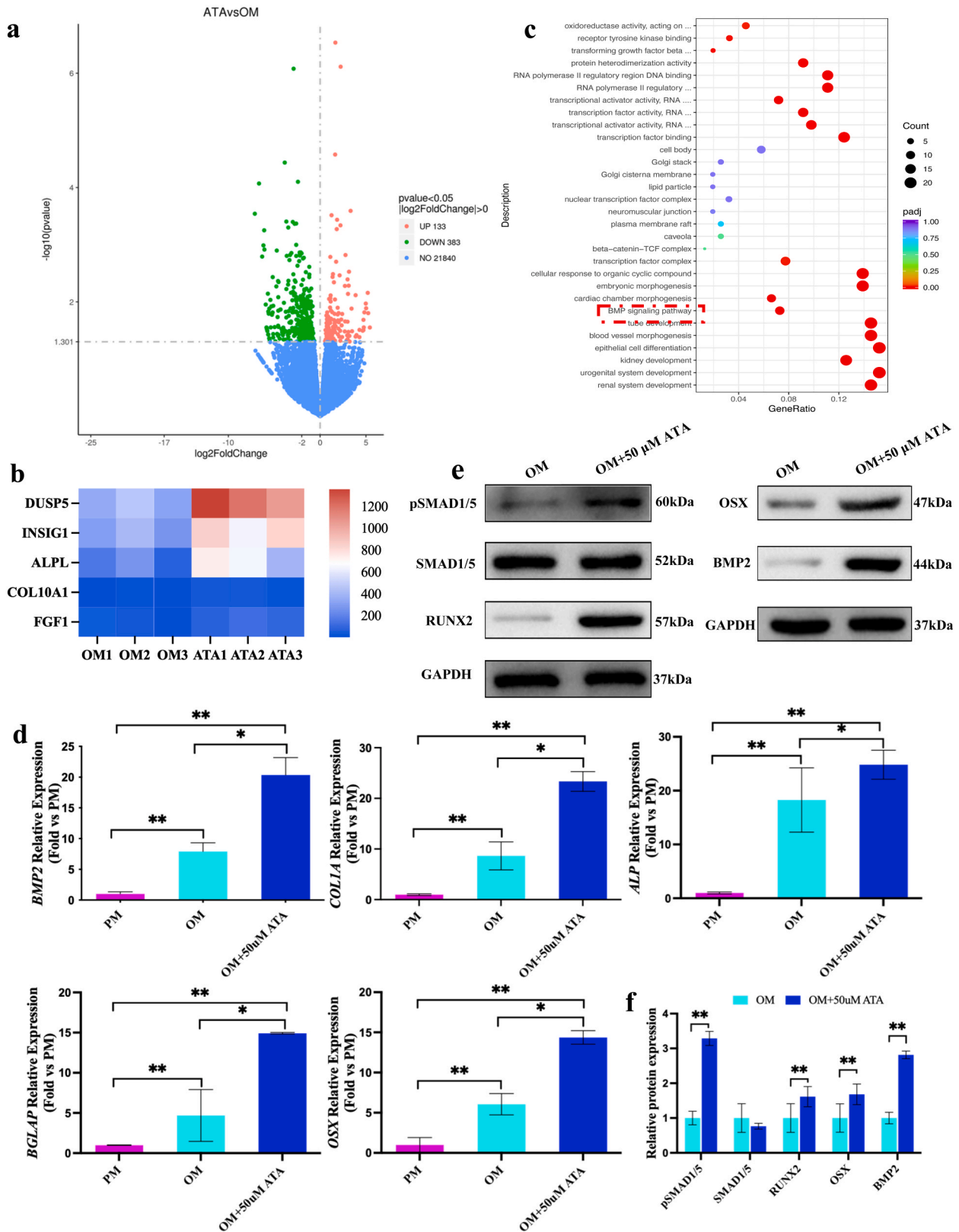


Fig. 3. Ataluren promoted hBMMSC osteogenic differentiation by activating the BMP-SMAD pathway. **a** Differential expression analysis results of RNA-seq data from hBMMSCs. **b** Upregulated genes showcased by RNA-seq between the ATA (ATA1, ATA2, and ATA3) and the OM (OM1, OM2 and OM3) groups. RNA seq was performed in triplicates. **c** GO enrichment analysis of DEGs using DAVID. **d** qRT-PCR for *BMP2*, *COL1A*, *ALP*, *BGLAP*, and *OSX*. **e** WB results for pSMAD1/5, SMAD1/5, RUNX2, OSX, BMP2, and the internal control GAPDH. **f** Quantitative analysis of WB. All data shown are the mean \pm SD in **e**, $n = 3$. * $P < 0.05$, ** $P < 0.01$ by ANOVA.

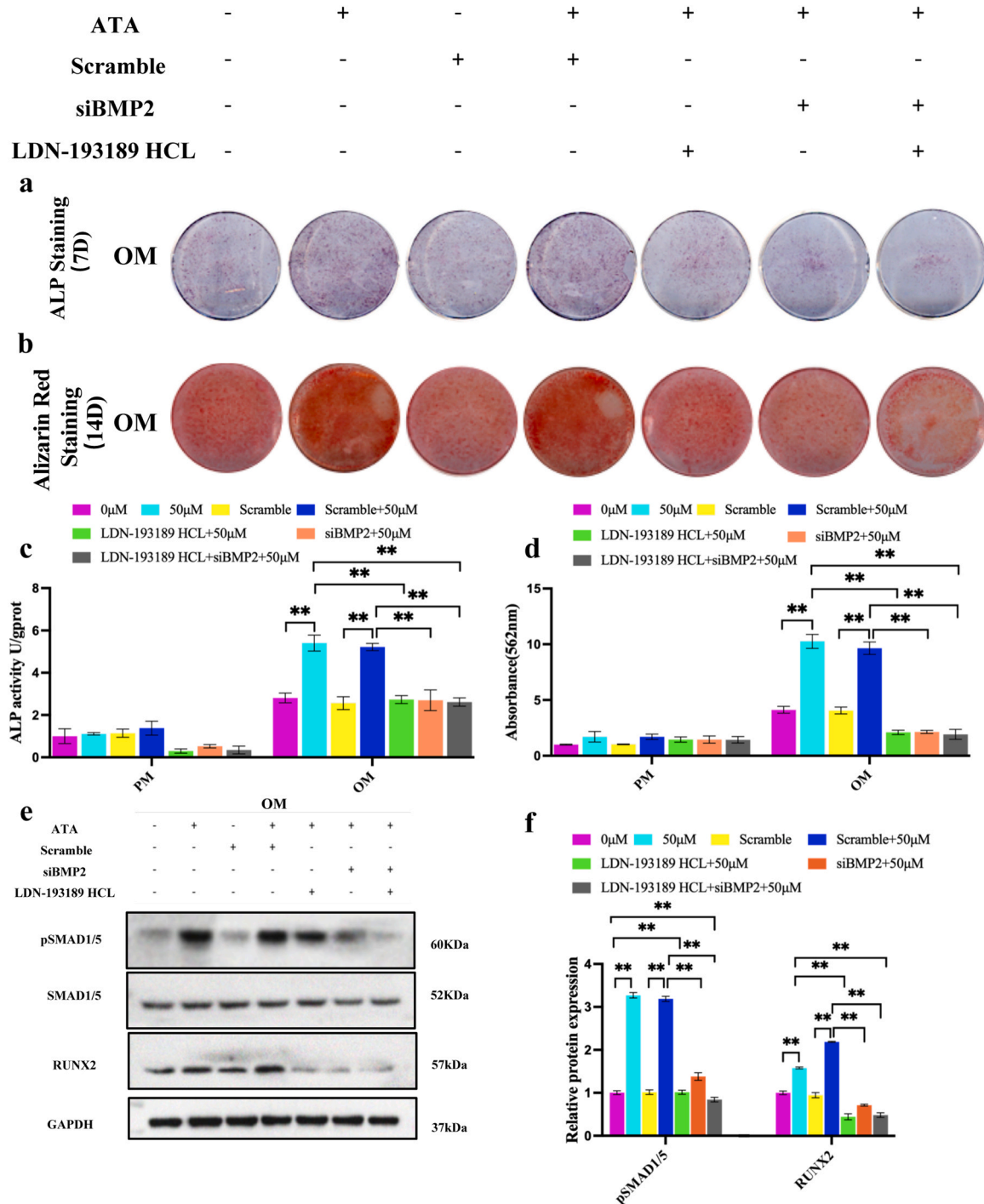


Fig. 4. The effect of ataluren on hBMMSC osteogenic differentiation which relies on the BMP-SMAD pathway. **a** ALP staining of hBMMSCs. **b** ARS staining of hBMMSCs. **c** The ALP activity quantification results. **d** The ARS semi-quantification results. **e** WB for the protein expression of SMAD1/5, pSMAD1/5, RUNX2, and the internal control GAPDH. **f** Quantitative analysis of WB. All data shown are the mean \pm SD in **c**, **d**, and **f**, $n = 3$. * $P < 0.05$, ** $P < 0.01$ by ANOVA.

treatment effectiveness in areas such as bone or cartilage [62]. Taken together, this evidence suggests that ataluren may act in the targeted management of hBMMSC osteogenic differentiation.

Furthermore, the transcriptome sequencing analysis results showed that 50 μ M ataluren upregulated DUSP5 most significantly, which elevated MSC osteogenic differentiation through the BMP-SMAD pathway, as demonstrated by our group before [43]. Besides, other research also suggested that DUSP5 overexpression inhibits NF- κ B pathway activation and thereby controls inflammation [63]. This may partially explain the decreased CTX-1 in the serum of OVX+ATA and

Aged+ATA mice. RNA-sequencing result showed that *FGF1*, *INDIG1* and *ALPL* were differential genes in ATA group. It has been shown that *FGF1* can directly stimulate *RUNX2* expression and increase its binding to promoters, leading to osteogenic differentiation [64,65]. However, we found in our validation study by qRT-PCR that the expression of *INDIG1* and *FGF1* was not significantly changed. *ALPL* is the downstream of the regulation of osteogenesis, although it is not in the BMP signaling pathway, and we verified by qRT-PCR that the expression of *ALPL* is significantly different. Based on this, we hypothesized that ataluren promotes osteogenesis by activating the BMP-SMAD pathway. Further

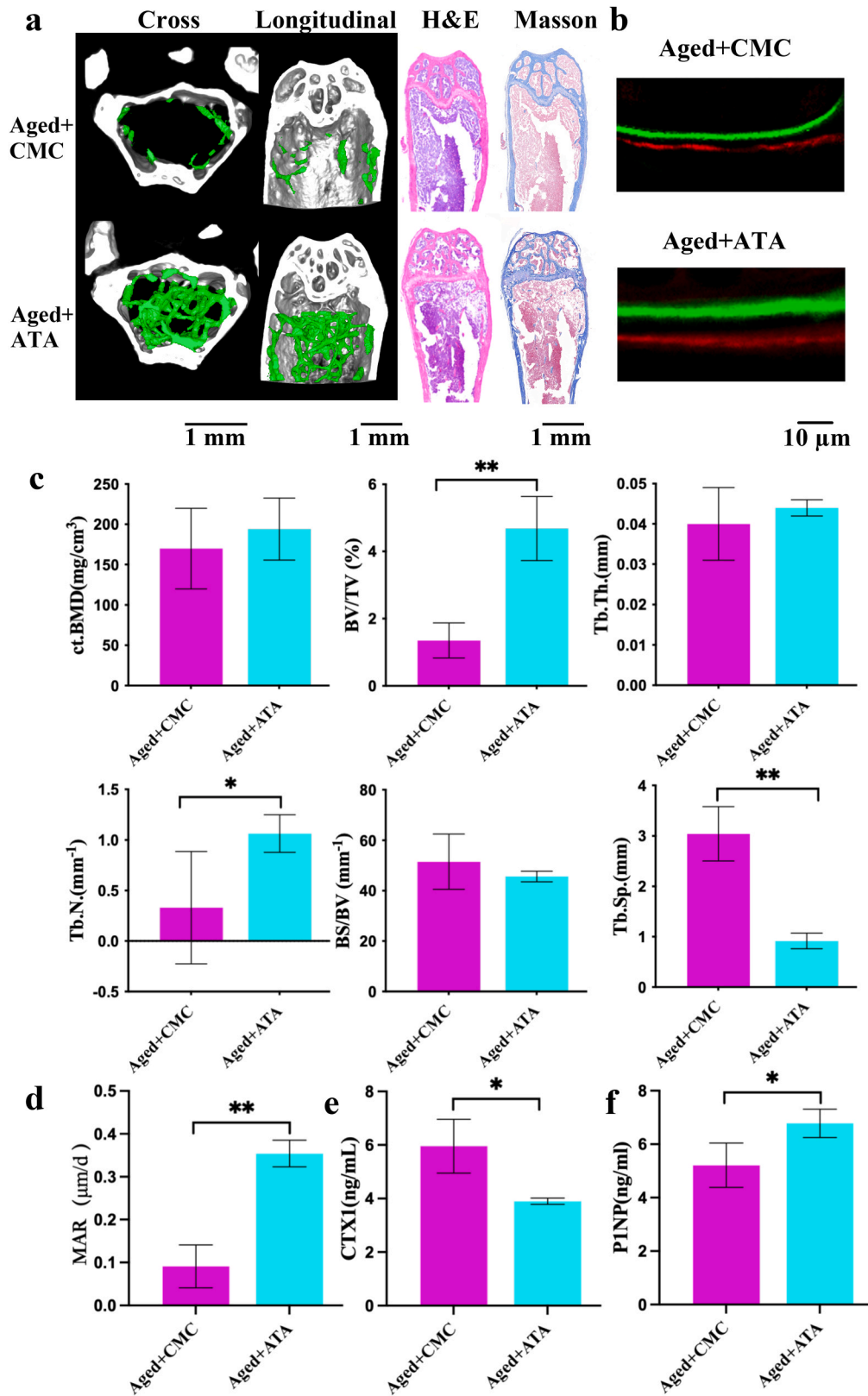


Fig. 5. Partially reversal of bone loss by ataluren in aged mice. **a** Micro-CT (left), H&E staining and Masson staining (right) images of Aged+CMC and Aged+ATA mice. Scale bar = 1 mm. **b** Representative images of new bone formation in the distal femoral epiphysis assessed by calcein and alizarin-3-methyliminodiacetic acid double-labeling. Scale bar = 10 μm. **c** BMD, BV/TV, BS/BV, Tb.Th, Tb.N, and Tb.Sp of Aged+CMC and Aged+ATA mice. **d** MAR of Aged+CMC and Aged+ATA mice. **e** Serum levels of CTX-1. **f** Serum levels of P1NP. All data shown are the mean ± SD in **c**, **d**, **e**, and **f**, n = 5. * *P* < 0.05, ** *P* < 0.01, when comparing with Aged+CMC control group by Student's *t* test.

exploration of the osteogenesis mechanisms showed that ataluren upgrades osteogenic differentiation by activating the BMP-SMAD signaling pathway. BMP2, a BMP family member, facilitates osteoblast differentiation by raising endocellular ALP activity and OCN and collagen synthesis and differentiation [66]. BMPs produce their effects by interacting with two BMP receptors (BMPRs). BMPRs exert their effects by interacting with extracellular BMPRs. BMPRs are activated by binding to extracellular BMP molecules [67,68]. A recent study demonstrated that 28.4 µg/mL ataluren improved BMPR2 protein expression in the R584X animal model and sectionally restored the BMPR2 protein index in endothelial cells extracted from patients carrying the R584X mutation [69]. In a study of hereditary pulmonary hypertension, WB on endothelial cell lysates treated with 5.7 µg/mL ataluren demonstrated 1.9- and 3.7-fold augmentation in BMPR2 protein expression and ligand-dependent phosphorylation of the downstream target gene SMADs, respectively [70]. Therefore, our results are consistent with previous reports. Nevertheless, our study indicates for the first time that ataluren facilitates osteogenesis via the BMP-SMAD signaling pathway. However, bone angiogenesis also plays an important role in bone formation. Previous study found that the pattern of vascular distribution along the cortex predicts the subsequent pattern of mineral deposition, which would implicate the key role of vasculature in bone morphogenesis [71,72]. While differentiation occurs in the corneal epithelium, RUNX1 maintains the epithelial cell fate [73]. Furthermore, evidences exhibited that RUNX1 plays a role in skeletal function [74,75]. Vascular morphogenesis and epithelium differentiation may be a potential research direction in GO analysis and need to be explored further in the future. Hence, although the mechanism of ataluren in promoting hBMMSC osteogenesis has not been clarified, it is mediated, at least in part, through BMP-SMAD signaling pathway activation.

Nonetheless, our study has some limitations. First, the results of both in vivo experiments (OVX and aging studies) indicated a reduction of bone resorption as evidenced by reduced CTX-1 levels. However, given that ataluren may be a pro-synthetic drug, we have not further determined the effect of ataluren on osteoclast differentiation and function, which warrants further exploration in future studies. Second, we did not determine the effect of ataluren on in vitro osteogenesis as studied by overexpression. Finally, we infer that the mechanism of increased bone formation in ataluren is activation of the BMP signaling pathway in hBMMSCs based on the results of in vitro experiments, which need to be further validated by in vivo intervention-based experiments.

5. Conclusions

DLEPS screening can identify new drug candidates for remedying osteoporosis. The screening representative compound ataluren prevented OVX-induced bone loss. Ataluren promoted osteogenic differentiation by increasing hBMMSC ALP activity and mineralization levels and increasing the mRNA and protein expression of osteogenic markers. Moreover, ataluren prevented bone loss caused by age-related conditions in mice. Mechanistically, ataluren promoted osteogenesis by activating the BMP-SMAD signaling pathway. Our study suggests that ataluren may be a therapeutic agent against osteoporosis by aiding hBMMSC osteogenic differentiation.

Funding source

This work was supported by the National Natural Science Foundation of China [grant number 81870742]; the Beijing Natural Science Foundation [grant numbers L222145, L182006]; Clinical Medicine Plus X - Young Scholars Project, Peking University, the Fundamental Research Funds for the Central Universities [grant number PKU2023LCXQ017].

CRedit authorship contribution statement

Lijun Zeng: Conceptualization, Data curation, Methodology, Formal

analysis, Writing-original draft, Writing-review & editing. **Ranli Gu:** Data curation, Formal analysis, Methodology, Resources, Validation. **Wei Li:** Methodology, Formal analysis, Writing-review & editing. **Yuzi Shao:** Methodology, Formal analysis, Writing-review & editing. **Yuan Zhu:** Methodology, Formal analysis, Writing-review & editing. **Zhengwei Xie:** Conceptualization, Methodology, Writing-review & editing. **Hao Liu:** Conceptualization, Methodology, Funding acquisition, Project administration, Writing-review & editing. **Yongsheng Zhou:** Conceptualization, Funding acquisition, Writing-review & editing, Supervision.

Declaration of Competing Interest

The authors declare that they have no known competing financial interests or personal relationships that could have appeared to influence the work reported in this paper..

Data Availability

Data will be made available on request.

Acknowledgements

We thank Dr. Xuejiao Liu for helpful advice to improve the experimental design.

Appendix A. Supporting information

Supplementary data associated with this article can be found in the online version at [doi:10.1016/j.biopha.2023.115332](https://doi.org/10.1016/j.biopha.2023.115332).

References

- [1] T.J. Aspray, T.R. Hill, Osteoporosis and the ageing skeleton, *Subcell. Biochem.* 91 (2019) 453–476, https://doi.org/10.1007/978-981-13-3681-2_16.
- [2] B. Langdahl, Treatment of postmenopausal osteoporosis with bone-forming and antiresorptive treatments: combined and sequential approaches, *Bone* 139 (2020), 115516, <https://doi.org/10.1016/j.bone.2020.115516>.
- [3] E.F. Eriksen, J. Halse, M.H. Moen, New developments in the treatment of osteoporosis, *Acta Obstet. Gynecol. Scand.* 92 (2013) 620–636, <https://doi.org/10.1111/j.1600-0412.2012.01473.x>.
- [4] L. Feller, N.H. Wood, R.A. Khammissa, U.M. Chikte, M. Bouckaert, J. Lemmer, Bisphosphonate-related osteonecrosis of the jaw, *Sadj* 66 (2011) 30–32.
- [5] C.A. Migliorati, M.A. Siegel, L.S. Elting, Bisphosphonate-associated osteonecrosis: a long-term complication of bisphosphonate treatment, *Lancet Oncol.* 7 (2006) 508–514, [https://doi.org/10.1016/s1470-2045\(06\)70726-4](https://doi.org/10.1016/s1470-2045(06)70726-4).
- [6] D. Tay, S. Cremers, J.P. Bilezikian, Optimal dosing and delivery of parathyroid hormone and its analogues for osteoporosis and hypoparathyroidism - translating the pharmacology, *Br. J. Clin. Pharmacol.* 84 (2018) 252–267, <https://doi.org/10.1111/bcp.13455>.
- [7] B.Z. Leder, Parathyroid hormone and parathyroid hormone-related protein analogs in osteoporosis therapy, *Curr. Osteoporos. Rep.* 15 (2017) 110–119, <https://doi.org/10.1007/s11914-017-0353-4>.
- [8] X.A. Qu, D.K. Rajpal, Applications of connectivity map in drug discovery and development, *Drug Discov. Today* 17 (2012) 1289–1298, <https://doi.org/10.1016/j.drudis.2012.07.017>.
- [9] J. Zhu, J. Wang, X. Wang, M. Gao, B. Guo, M. Gao, J. Liu, Y. Yu, L. Wang, W. Kong, Y. An, Z. Liu, X. Sun, Z. Huang, H. Zhou, N. Zhang, R. Zheng, Z. Xie, Prediction of drug efficacy from transcriptional profiles with deep learning, *Nat. Biotechnol.* 39 (2021) 1–9, <https://doi.org/10.1038/s41587-021-00946-z>.
- [10] H. Jiang, C. Hu, M. Chen, The advantages of connectivity map applied in traditional Chinese medicine, *Front. Pharmacol.* 12 (2021), 474267, <https://doi.org/10.3389/fphar.2021.474267>.
- [11] B. Short, N. Brouard, T. Occhiodoro-Scott, A. Ramakrishnan, P.J. Simmons, Mesenchymal stem cells, *Arch. Med. Res.* 34 (2003) 565–571, <https://doi.org/10.1016/j.arcmed.2003.09.007>.
- [12] R. Baron, M. Kneissel, WNT signaling in bone homeostasis and disease: from human mutations to treatments, *Nat. Med.* 19 (2013) 179–192, <https://doi.org/10.1038/nm.3074>.
- [13] N.G.M. Thielen, P.M. van der Kraan, A.P.M. van Caam, TGFβ/BMP signaling pathway in cartilage homeostasis, *Cells* 8 (2019) 69–99, <https://doi.org/10.3390/cells8090969>.
- [14] M. Hettiaratchi, L. Krishnan, T. Rouse, C. Chou, T. McDevitt, R. Gulberg, Heparin-mediated delivery of bone morphogenetic protein-2 improves spatial localization of bone regeneration, *Sci. Adv.* 6 (2020), eaay1240, <https://doi.org/10.1126/sciadv.aay1240>.

- [15] G. Chen, C. Deng, Y.P. Li, TGF- β and BMP signaling in osteoblast differentiation and bone formation, *Int. J. Biol. Sci.* 8 (2012) 272–288, <https://doi.org/10.7150/ijbs.2929>.
- [16] K. Tezuka, M. Yasuda, N. Watanabe, N. Morimura, K. Kuroda, S. Miyatani, N. Hozumi, Stimulation of osteoblastic cell differentiation by Notch, *J. Bone Min. Res.* 17 (2002) 231–239, <https://doi.org/10.1359/jbmr.2002.17.2.231>.
- [17] F. Milat, K.W. Ng, Is Wnt signalling the final common pathway leading to bone formation? *Mol. Cell Endocrinol.* 310 (2009) 52–62, <https://doi.org/10.1016/j.mce.2009.06.002>.
- [18] M. Majidinia, A. Sadeghpour, B. Yousefi, The roles of signaling pathways in bone repair and regeneration, *J. Cell. Physiol.* 233 (2018) 2937–2948, <https://doi.org/10.1002/jcp.26042>.
- [19] J. Lu, H. Zhang, J. Pan, Z. Hu, L. Liu, Y. Liu, X. Yu, X. Bai, D. Cai, H. Zhang, Fargesin ameliorates osteoarthritis via macrophage reprogramming by downregulating MAPK and NF- κ B pathways, *Arthritis Res. Ther.* 23 (2021), 142, <https://doi.org/10.1186/s13075-021-02512-z>.
- [20] S.K. Ramasamy, A.P. Kusumbe, L. Wang, R.H. Adams, Endothelial Notch activity promotes angiogenesis and osteogenesis in bone, *Nature* 507 (2014) 376–380, <https://doi.org/10.1038/nature13146>.
- [21] T. Komori, Regulation of bone development and extracellular matrix protein genes by RUNX2, *Cell Tissue Res.* 339 (2010) 189–195, <https://doi.org/10.1007/s00441-009-0832-8>.
- [22] T. Katagiri, T. Watabe, Bone morphogenetic proteins, *Cold Spring Harb. Perspect. Biol.* 8 (2016), a021899, <https://doi.org/10.1101/cshperspect.a021899>.
- [23] K. Bushby, R. Finkel, B. Wong, R. Barohn, C. Campbell, G.P. Comi, A.M. Connolly, J.W. Day, K.M. Flanigan, N. Goemans, K.J. Jones, E. Mercuri, R. Quinlivan, J. B. Renfroe, B. Russman, M.M. Ryan, M. Tulinius, T. Voit, S.A. Moore, H. Lee Sweeney, R.T. Abresch, K.L. Coleman, M. Eagle, J. Florence, E. Gappmaier, A. M. Glanzman, E. Henricson, J. Barth, G.L. Elfring, A. Reha, R.J. Spiegel, M. W. O'Donnell, S.W. Peltz, C.M. McDonald, Ataluren treatment of patients with nonsense mutation dystrophinopathy, *Muscle Nerve* 50 (2014) 477–487, <https://doi.org/10.1002/mus.24332>.
- [24] S. Hirawat, E.M. Welch, G.L. Elfring, V.J. Northcutt, S. Paushkin, S. Hwang, E. M. Leonard, N.G. Almstead, W. Ju, S.W. Peltz, L.L. Miller, Safety, tolerability, and pharmacokinetics of PTC124, a nonaminoglycoside nonsense mutation suppressor, following single- and multiple-dose administration to healthy male and female adult volunteers, *J. Clin. Pharmacol.* 47 (2007) 430–444, <https://doi.org/10.1177/0091270006297140>.
- [25] C. Campbell, R.J. Barohn, E. Bertini, B. Chabrol, G.P. Comi, B.T. Darras, R. S. Finkel, K.M. Flanigan, N. Goemans, S.T. Iannaccone, K.J. Jones, J. Kirschner, J. K. Mah, K.D. Mathews, C.M. McDonald, E. Mercuri, Y. Nevo, Y. Péron, J. B. Renfroe, M.M. Ryan, J.B. Sampson, U. Schara, T. Sejersen, K. Selby, M. Tulinius, J.J. Vilchez, T. Voit, L.J. Wei, B.L. Wong, G. Elfring, M. Souza, J. McIntosh, P. Trifillis, S.W. Peltz, F. Muntoni, Meta-analyses of ataluren randomized controlled trials in nonsense mutation Duchenne muscular dystrophy, *J. Comp. Eff. Res.* 9 (2020) 973–984, <https://doi.org/10.2217/ce-2020-0095>.
- [26] J. Berger, M. Li, S. Berger, M. Meilak, J. Rientjes, P.D. Currie, Effect of Ataluren on dystrophin mutations, *J. Cell. Mol. Med.* 24 (2020) 6680–6689, <https://doi.org/10.1111/jcmm.15319>.
- [27] S. Aravind, Rajiv Narayan, M. Steven, A next generation connectivity map: 11000 platform and the first 1,000,000 profiles, *Cell* 171 (2017) 1437–1452, <https://doi.org/10.1016/j.cell.2017.10.049>.
- [28] M.J. Kusner, Paige B., Hernández-Lobato J.M., Grammar Variational Autoencoder, (2017).
- [29] M. Garber, M.G. Grabherr, M. Guttman, C. Trapnell, Computational methods for transcriptome annotation and quantification using RNA-seq, *Nat. Methods* 8 (2011), <https://doi.org/10.1038/nmeth.1613>.
- [30] N.L. Bray, H. Pimentel, P. Melsted, L. Pachter, Near-optimal RNA-Seq quantification, *Comput. Sci.* (2015) 1–21, <https://doi.org/10.48550/arXiv.1505.02710>.
- [31] R. Kong, J. Ma, S. Hwang, E. Goodwin, V. Northcutt, J. Babiak, N. Almstead, J. McIntosh, Metabolism and disposition of ataluren after oral administration to mice, rats, dogs, and humans, *Drug Metab. Dispos.* 48 (2020) 317–325, <https://doi.org/10.1124/dmd.119.089391>.
- [32] S. Movérare-Skrtric, J. Wu, P. Henning, K.L. Gustafsson, K. Sjögren, S.H. Windahl, A. Koskela, J. Tuukkanen, A.E. Börjesson, M.K. Lagerquist, U.H. Lerner, F.P. Zhang, J. Gustafsson, M. Poutanen, C. Ohlsson, The bone-sparing effects of estrogen and WNT16 are independent of each other, *Proc. Natl. Acad. Sci. USA* 112 (2015) 14972–14977, <https://doi.org/10.1073/pnas.1520408112>.
- [33] N. Lian, T. Lin, W. Liu, W. Wang, L. Li, S. Sun, J.S. Nyman, X. Yang, Transforming growth factor β suppresses osteoblast differentiation via the vimentin activating transcription factor 4 (ATF4) axis, *J. Biol. Chem.* 287 (2012) 35975–35984, <https://doi.org/10.1074/jbc.M112.372458>.
- [34] N.A. Hanson, C.M. Bagi, Alternative approach to assessment of bone quality using micro-computed tomography, *Bone* 35 (2004) 326–333, <https://doi.org/10.1016/j.bone.2004.02.019>.
- [35] J. Yan, J.W. Herzog, K. Tsang, C.A. Brennan, M.A. Bower, W.S. Garrett, B.R. Sartor, A.O. Aliprantis, J.F. Charles, Gut microbiota induce IGF-1 and promote bone formation and growth, *Proc. Natl. Acad. Sci. USA* 113 (2016) E7554–e7563, <https://doi.org/10.1073/pnas.1607235113>.
- [36] M.L. Bouxsein, S.K. Boyd, B.A. Christiansen, R.E. Guldborg, K.J. Jepsen, R. Müller, Guidelines for assessment of bone microstructure in rodents using micro-computed tomography, *J. Bone Min. Res.* 25 (2010) 1468–1486, <https://doi.org/10.1002/jbmr.141>.
- [37] P. Benisch, T. Schilling, L. Klein-Hitpass, S.P. Frey, L. Seefried, N. Raaijmakers, M. Krug, M. Regensburger, S. Zeck, T. Schinke, M. Amling, R. Ebert, F. Jakob, The transcriptional profile of mesenchymal stem cell populations in primary osteoporosis is distinct and shows overexpression of osteogenic inhibitors, *PLoS One* 7 (2012), e45142, <https://doi.org/10.1371/journal.pone.0045142>.
- [38] A. Lekturm Alpan, M. Çalişir, A. Kızıldağ, M. Özdede, Ö. Özmen, Effects of a glycogen synthase kinase 3 inhibitor tideglusib on bone regeneration with calvarial defects, *J. Craniofac. Surg.* (2020) 1477–1482, <https://doi.org/10.1097/scs.0000000000006326>.
- [39] E.J. Lee, M.K. Kang, Y.H. Kim, D.Y. Kim, H. Oh, S.I. Kim, S.Y. Oh, W. Na, Y. H. Kang, Coumarin ameliorates impaired bone turnover by inhibiting the formation of advanced glycation end products in diabetic osteoblasts and osteoclasts, *Biomolecules* 10 (2020) 52–62, <https://doi.org/10.3390/biom10071052>.
- [40] J.C. Stevenson, P. Teter, B. Lees, 17 β -estradiol (1 mg/day) continuously combined with hydrogesterone (5, 10 or 20 mg/day) increases bone mineral density in postmenopausal women, *Maturitas* 38 (2001) 197–203, [https://doi.org/10.1016/s0378-5122\(00\)00219-x](https://doi.org/10.1016/s0378-5122(00)00219-x).
- [41] S.R. Nahorski, *The pharmacological basis of therapeutics*, *Trends Pharmacol. Sci.* (1990).
- [42] T.H. Saleem, N. Abo El-Maali, M.H. Hassan, N.A. Mohamed, N.A.M. Mostafa, E. Abdel-Kahaar, A.S. Tammam, Comparative protective effects of N-acetylcysteine, N-acetyl methionine, and N-acetyl glucosamine against paracetamol and phenacetin therapeutic doses-induced hepatotoxicity in rats, *Int. J. Hepatol.* 2018 (2018), 7603437, <https://doi.org/10.1155/2018/7603437>.
- [43] X. Liu, X. Liu, Y. Du, M. Hu, Y. Tian, Z. Li, L. Lv, X. Zhang, Y. Liu, Y. Zhou, P. Zhang, DUSP5 promotes osteogenic differentiation through SCP1/2-dependent phosphorylation of SMAD1, *Stem Cells* 39 (2021) 1395–1409, <https://doi.org/10.1002/stem.3428>.
- [44] R. Wang, M. Shi, F. Xu, Y. Qiu, P. Zhang, K. Shen, Q. Zhao, J. Yu, Y. Zhang, Graphdiyne-modified TiO₂ nanofibers with osteoinductive and enhanced photocatalytic antibacterial activities to prevent implant infection, *Nat. Commun.* 11 (2020), 4465, <https://doi.org/10.1038/s41467-020-18267-1>.
- [45] L. Wang, H. Yang, J. Huang, S. Pei, L. Wang, J.Q. Feng, D. Jing, H. Zhao, H. M. Kronenberg, D.C. Moore, Targeted Ptpn11 deletion in mice reveals the essential role of SHP2 in osteoblast differentiation and skeletal homeostasis, *Bone Res* 9 (2021), 6, <https://doi.org/10.1038/s41413-020-00129-7>.
- [46] Q. Gan, L. Chen, H.P. Bei, S.W. Ng, H. Guo, G. Liu, H. Pan, C. Liu, X. Zhao, Z. Zheng, Artificial cilia for soft and stable surface covalent immobilization of bone morphogenetic protein-2, *Bioact. Mater.* 24 (2023) 551–562, <https://doi.org/10.1016/j.bioactmat.2022.12.029>.
- [47] W. Chen, S.S. Foo, E. Hong, C. Wu, J.U. Jung, Zika virus NS3 protease induces bone morphogenetic protein-dependent brain calcification in human fetuses, *Nat. Microbiol.* 6 (2021) 455–466, <https://doi.org/10.1038/s41564-020-00850-3>.
- [48] G. Yu, L. Wang, Y. Li, Z. Ma, Y. Li, Identification of drug candidate for osteoporosis by computational bioinformatics analysis of gene expression profile, *Eur. J. Med. Res.* 18 (2013), 5, <https://doi.org/10.1186/2047-783x-18-5>.
- [49] A.M. Brum, J. van de Peppel, C.S. van der Leijde, M. Schreuders-Koedam, M. Eijken, B.C. van der Eerden, J.P. van Leeuwen, Connectivity Map-based discovery of parabendazole reveals targetable human osteogenic pathway, *Proc. Natl. Acad. Sci. USA* 112 (2015) 12711–12716, <https://doi.org/10.1073/pnas.1501597112>.
- [50] P. Zhao, C.G. Mangleburg, I. Al-Ramahi, J. Botas, J.M. Shulman, Systems genetic dissection of Alzheimer's disease brain gene expression networks, *Alzheimers Dement* 17 (2) (2021), e058716, <https://doi.org/10.1002/alz.058716>.
- [51] R. Hajjo, V. Setola, B.L. Roth, A. Tropsha, Chemocentric informatics approach to drug discovery: identification and experimental validation of selective estrogen receptor modulators as ligands of 5-hydroxytryptamine-6 receptors and as potential cognition enhancers, *J. Med. Chem.* 55 (2012) 5704–5719, <https://doi.org/10.1021/jm2011657>.
- [52] E. Ali, M. Wu, L. Xiao-Li, K. Chee-Keong, Computational prediction of drug–target interactions using chemogenomic approaches: an empirical survey, *Brief. Bioinform.* 20 (2019) 1337–1357, <https://doi.org/10.1093/bib/bby002>.
- [53] J.M. Stokes, K. Yang, K. Swanson, W. Jin, A. Cubillos-Ruiz, N.M. Donghia, C. R. MacNair, S. French, L.A. Carfrae, Z. Bloom-Ackermann, V.M. Tran, A. Chiappino-Pepe, A.H. Badran, I.W. Andrews, E.J. Chory, G.M. Church, E. D. Brown, T.S. Jaakkola, R. Barzilay, J.J. Collins, A deep learning approach to antibiotic discovery, 688-702.e613, *Cell* 180 (2020), <https://doi.org/10.1016/j.cell.2020.01.021>.
- [54] T.T. Ashburn, K.B. Thor, Drug repositioning: identifying and developing new uses for existing drugs, *Nat. Rev. Drug Discov.* 3 (2004) 673–683, <https://doi.org/10.1038/nrd1468>.
- [55] M.J. Keiser, V. Setola, J.J. Irwin, C. Laggner, A.I. Abbas, S.J. Hufeisen, N.H. Jensen, M.B. Kujler, R.C. Matos, T.B. Tran, R. Whaley, R.A. Glennon, J. Hert, K.L. Thomas, D.D. Edwards, B.K. Shoichet, B.L. Roth, Predicting new molecular targets for known drugs, *Nature* 462 (2009) 175–181, <https://doi.org/10.1038/nature08506>.
- [56] R.S. Finkel, Read-through strategies for suppression of nonsense mutations in Duchenne/Becker muscular dystrophy: aminoglycosides and ataluren (PTC124), *J. Child Neurol.* 25 (2010) 1158–1164, <https://doi.org/10.1177/0883073810371129>.
- [57] A.A. Aslam, C. Higgins, I.P. Sinha, K.W. Southern, Ataluren and similar compounds (specific therapies for premature termination codon class I mutations) for cystic fibrosis, *Cochrane Database Syst. Rev.* (1) (2017), Cd012040, <https://doi.org/10.1002/14651858.Cd012040.pub2>.
- [58] J.J. Porter, C.S. Heil, J.D. Lueck, Therapeutic promise of engineered nonsense suppressor tRNAs, *Wiley Interdiscip. Rev. RNA* 12 (2021), e1641, <https://doi.org/10.1002/wrna.1641>.
- [59] R. Kong, J. Ma, S. Hwang, Y.C. Moon, E.M. Welch, M. Weetall, J.M. Colacino, N. Almstead, J. Babiak, E. Goodwin, In vitro metabolism, reaction phenotyping,

- enzyme kinetics, CYP inhibition and induction potential of ataluren, *Pharm. Res. Perspect.* 8 (2020), e00576, <https://doi.org/10.1002/prp2.576>.
- [60] M.Y. Ng, H. Li, M.D. Ghelfi, Y.E. Goldman, B.S. Cooperman, Ataluren and aminoglycosides stimulate read-through of nonsense codons by orthogonal mechanisms, *Proc. Natl. Acad. Sci. USA* 118 (2021), <https://doi.org/10.1073/pnas.2020599118>.
- [61] B. Roy, W.J. Friesen, Y. Tomizawa, J.D. Leszyk, J. Zhuo, B. Johnson, J. Dakka, C. R. Trotta, X. Xue, V. Mutyam, K.M. Keeling, J.A. Mobley, S.M. Rowe, D.M. Bedwell, E.M. Welch, A. Jacobson, Ataluren stimulates ribosomal selection of near-cognate tRNAs to promote nonsense suppression, *Proc. Natl. Acad. Sci. USA* 113 (2016) 12508–12513, <https://doi.org/10.1073/pnas.1605336113>.
- [62] R. Bartolomeo, E.V. Polishchuk, N. Volpi, R.S. Polishchuk, A. Auricchio, Pharmacological read-through of nonsense ARSB mutations as a potential therapeutic approach for mucopolysaccharidosis VI, *J. Inher. Metab. Dis.* 36 (2013) 363–371, <https://doi.org/10.1007/s10545-012-9521-y>.
- [63] Z. Wu, L. Xu, Y. He, K. Xu, Z. Chen, S.A.A. Moqbel, C. Ma, L. Jiang, J. Ran, L. Wu, Y. Zhong, DUSP5 suppresses interleukin-1 β -induced chondrocyte inflammation and ameliorates osteoarthritis in rats, *Aging* 12 (2020) 26029–26046, <https://doi.org/10.18632/aging.202252>.
- [64] F. Kidwai, B.W.H. Mui, D. Arora, K. Iqbal, M. Hockaday, L.F. de Castro Diaz, N. Cherman, D. Martin, V.D. Myneni, M. Ahmad, K. Futrega, S. Ali, R.K. Merling, D. S. Kaufman, J. Lee, P.G. Robey, Lineage-specific differentiation of osteogenic progenitors from pluripotent stem cells reveals the FGF1-RUNX2 association in neural crest-derived osteoprogenitors, *Stem Cells* 38 (2020) 1107–1123, <https://doi.org/10.1002/stem.3206>.
- [65] T. Komori, Molecular mechanism of Runx2-dependent bone development, *Mol. Cells* 43 (2020) 168–175, <https://doi.org/10.14348/molcells.2019.0244>.
- [66] M. Wu, G. Chen, Y.P. Li, TGF- β and BMP signaling in osteoblast, skeletal development, and bone formation, homeostasis and disease, *Bone Res.* 4 (2016), 16009, <https://doi.org/10.1038/boneres.2016.9>.
- [67] A.C. Carreira, G.G. Alves, W.F. Zambuzzi, M.C. Sogayar, J.M. Granjeiro, Bone morphogenetic proteins: structure, biological function and therapeutic applications, *Arch. Biochem. Biophys.* 561 (2014) 64–73, <https://doi.org/10.1016/j.abb.2014.07.011>.
- [68] T.K. Sampath, A.H. Reddi, Discovery of bone morphogenetic proteins - a historical perspective, *Bone* 140 (2020), 115548, <https://doi.org/10.1016/j.bone.2020.115548>.
- [69] L. Long, X. Yang, M. Southwood, S. Moore, A. Crosby, P.D. Upton, B.J. Dunmore, N. W. Morrell, Targeting translational read-through of premature termination mutations in BMPR2 with PTC124 for pulmonary arterial hypertension, 2045894020935783, *Pulm. Circ.* 10 (2020), <https://doi.org/10.1177/2045894020935783>.
- [70] K.M. Drake, B.J. Dunmore, L.N. McNelly, N.W. Morrell, M.A. Aldred, Correction of nonsense BMPR2 and SMAD9 mutations by ataluren in pulmonary arterial hypertension, *Am. J. Respir. Cell. Mol. Biol.* 49 (2013) 403–409, <https://doi.org/10.1165/rcmb.2013-01000C>.
- [71] A. Ben Shoham, C. Rot, T. Stern, S. Krief, A. Akiva, T. Dadosh, H. Sabany, Y. Lu, K. E. Kadler, E. Zelzer, Deposition of collagen type I onto skeletal endothelium reveals a new role for blood vessels in regulating bone morphology, *Development* 143 (2016) 3933–3943, <https://doi.org/10.1242/dev.139253>.
- [72] A. Sharif, T. Stern, C. Rot, R. Shahar, E. Zelzer, Muscle force regulates bone shaping for optimal load-bearing capacity during embryogenesis, *Development* 138 (2011) 3247–3259, <https://doi.org/10.1242/dev.063768>.
- [73] M. Li, H. Huang, L. Li, C. He, L. Zhu, H. Guo, L. Wang, J. Liu, S. Wu, J. Liu, T. Xu, Z. Mao, N. Cao, K. Zhang, F. Lan, J. Ding, J. Yuan, Y. Liu, H. Ouyang, Core transcription regulatory circuitry orchestrates corneal epithelial homeostasis, *Nat. Commun.* 12 (2021), 420, <https://doi.org/10.1038/s41467-020-20713-z>.
- [74] I. Antony-Debré, V.T. Manchev, N. Balayn, D. Bluteau, C. Tomowiak, C. Legrand, T. Langlois, O. Bawa, L. Tosca, G. Tachdjian, B. Leheup, N. Debili, I. Plo, J.A. Mills, D.L. French, M.J. Weiss, E. Solary, R. Favier, W. Vainchenker, H. Raslova, Level of RUNX1 activity is critical for leukemic predisposition but not for thrombocytopenia, *Blood* 125 (2015) 930–940, <https://doi.org/10.1182/blood-2014-06-585513>.
- [75] Y.H. Hsu, K. Estrada, E. Evangelou, C. Ackert-Bicknell, K. Akesson, T. Beck, S. J. Brown, T. Capellini, L. Carbone, J. Cauley, C.L. Cheung, S.R. Cummings, S. Czerwinski, S. Demissie, M. Econs, D. Evans, C. Farber, K. Gautvik, T. Harris, C. Kammerer, J. Kemp, D.L. Koller, A. Kung, D. Lawlor, M. Lee, M. Lorentzon, F. McGuigan, C. Medina-Gomez, B. Mitchell, A. Newman, C. Nielson, C. Ohlsson, M. Peacock, S. Reppe, J.B. Richards, J. Robbins, G. Sigurdsson, T.D. Spector, K. Stefansson, E. Streeten, U. Styrkarsdottir, J. Tobias, K. Trajanoska, A. Uitterlinden, L. Vandenput, S.G. Wilson, L. Yerges-Armstrong, M. Young, M. C. Zillikens, F. Rivadeneira, D.P. Kiel, D. Karasik, Meta-analysis of genomewide association studies reveals genetic variants for hip bone geometry, *J. Bone Min. Res.* 34 (2019) 1284–1296, <https://doi.org/10.1002/jbmr.3698>.